Opto-Electronic Advances

Article

June 2023, Vol. 6, No. 6

DOI: 10.29026/oea.2023.220170

# Hot electron electrochemistry at silver activated by femtosecond laser pulses

Oskar Armbruster[1,2]*, Hannes Pöhl[2] and Wolfgang Kautek[2]*

A silver microelectrode with a diameter of 30 µm in an aqueous $K_2SO_4$ electrolyte was irradiated with 55 fs and 213 fs laser pulses. This caused the emission of electrons which transiently charged the electrochemical double layer. The two applied pulse durations were significantly shorter than the electron-phonon relaxation time. The laser pulse durations had negligible impact on the emitted charge, which is incompatible with multiphoton emission. On the other hand, the observed dependence of emitted charge on laser fluence and electrode potential supports the thermionic emission mechanism.

**Keywords:** hot electron emission; femtosecond laser; laser electrochemistry; silver electrode

Armbruster O, Pöhl H, Kautek W. Hot electron electrochemistry at silver activated by femtosecond laser pulses. *Opto-Electron Adv* **6**, 220170 (2023).

## Introduction

The photoelectric effect describes the ejection of an electron from a metal by a high-energy photon (photon energy > work function of the metal)[1,2]. High intensity irradiation with low-energy photons can also result in electron emission by the multiphoton photoelectric effect[3–6].

Additionally, low-energy photons can generate hot electrons which are in thermal nonequilibrium with the host lattice[7–9]. Electron-electron scattering leads to equilibration on a sub-picosecond time scale, which allows the application of the two-temperature model[10]. After the electron-phonon relaxation time, which is on the order of several picoseconds, electrons return to thermal equilibrium with the lattice by electron-phonon-scattering. Due to the comparatively low heat capacity of the electron gas, electron temperatures of the order of $10^3$ K to $10^4$ K are easily achieved while maintaining a cold lattice. These hot electrons can be thermally emitted into the environment as a current burst with a duration on the order of the electron-phonon relaxation time[11–13].

For a Gaussian beam, the absorbed volumetric energy density is

$$U(r,z) = \frac{2\,\beta\,E}{w^2\,\pi\,\mu}\exp\left(-2\left(\frac{r}{w}\right)^2\right)\exp\left(-\frac{z}{\mu}\right), \quad (1)$$

where $E$ is the pulse energy, $\beta$ is the fraction of absorbed radiation, $w$ is the Gaussian beam radius, and $\mu$ = 142 nm is the effective absorption length of silver[8]. For low electron temperatures up to some 5000 K, the electron heat capacity of silver $C_e$ is approximately $C_e \approx \gamma_e T_e$[14] where $\gamma_e$ = 62.8 J m$^{-3}$ K$^{-2}$ is the heat capacitance coefficient of silver[14]. Via $C_e = \mathrm{d}U/\mathrm{d}T_e$, the electron temperature $T_e$ thus is

$$T_e(r,z) = \sqrt{\frac{2\,U(r,z)}{\gamma_e}}. \quad (2)$$

Figure 1 shows the electron temperature calculated according to Eq. (2).

[1]University of Natural Resources and Life Sciences, Vienna, Department of Bionanosciences, Muthgasse 11, 1190 Vienna, Austria; [2]University of Vienna, Department of Physical Chemistry, Währinger Straße 42, 1090 Vienna, Austria.

*Correspondence: O Armbruster, E-mail: oskar.armbruster@boku.ac.at; W Kautek, E-mail: wolfgang.kautek@univie.ac.at

Received: 24 August 2022; Accepted: 16 January 2023; Published online: 31 March 2023

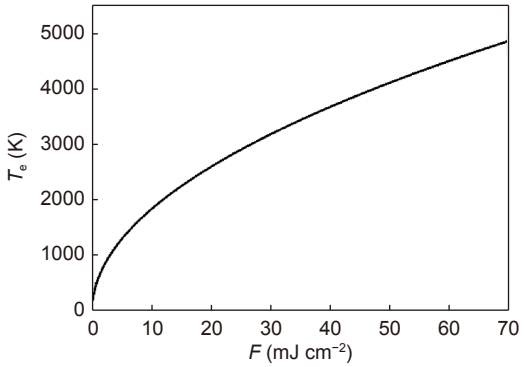


**Fig. 1 | Calculated electron temperature $T_e$ of silver for various incident laser fluences $F$ according to Equation (2) with $\gamma_e$ = 62.8 J m$^{-3}$ K$^{-2}$, $\mu$ = 142 nm, and $\beta$ = 0.15.**

A metal under irradiation in contact with an electrolyte emits electrons which undergo thermalization and solvation within a time span of 100 fs to 1 ps corresponding to the fast Debye relaxation time in water[15]. In an electron acceptor-free solution, solvated electrons may then diffuse back to the electrode and are reinjected. If, however, a sufficient number of electron acceptors (such as $H_3O^+$, $N_2O$, or $NO_3^-$) are present, the electrons can be scavenged[16].

The work function from a metallic electrode into an electrolyte solution $\phi$ is the difference between the conduction band edge of the solution and the Fermi energy of the metal. $\phi$ depends on the electrode potential $\varphi$ versus a reference potential and on the work function at that reference potential $\phi_0$ so that

$$\phi = \phi_0 + q_e\,\varphi\ , \tag{3}$$

with the elementary charge $q_e$.

Thermionic electron emission from a heated electron gas in nonequilibrium with the host lattice has been calculated using a one-dimensional interface potential[17]. The emitted charge density $q$ is mainly determined by the electron gas temperature $T_e$ at the surface and the electrode potential contained in the work function[17]. At $T_e < T_c$ (~ 1500 K[11]) tunneling is predominant, whereas at $T_e > T_c$ over the barrier emission prevails[17]. When $T_e > T_c$, the charge emitted from the electron gas into the electrolyte is

$$q \approx A_0\ T_e^2 \frac{k_B\ T_e}{\phi} \tau_e\ \exp\left(-\frac{\phi}{k_B\ T_e}\right)\ , \tag{4}$$

with the Richardson constant $A_0 \approx 120$ A cm$^{-2}$ K$^{-1}$, the Boltzmann constant $k_B$, the duration of the current pulse which is equal to the electron-phonon relaxation time $\tau_e$, and the work function in an electrolyte $\phi$ (Eq. (3)). Equation (4) describes the exponential dependence of $q$ on the pulse energy $E$ (Eqs. (1) and (2)) and the electrode potential $\varphi$ (Eq. (3)). In the tunneling case, $T_e < T_c$, the emitted charge is negligible and cannot be measured experimentally[17].

Due to the Gaussian laser beam shape, the electron temperature $T_e$ and hence the emitted charge density $q$ is radially nonconstant. Hence, the total emitted charge $Q$ is

$$Q = 2\pi \int_0^{r_e} q\ r\ \mathrm{d}r\ , \tag{5}$$

where $r_e$ is the electrode radius.

At relatively high electrolyte concentrations, the electrochemical diffuse double-layer can be neglected. The latter represents the space charge in the electrolyte[18].

There has been vivid interest in laser electrochemical phenomena and applications. Laser-induced electrochemical deposition of metals on metals relies possibly on thermal and defect generation effects[19]. When semiconductor substrates are chosen, locally photogenerated electrons can reduce metal ions resulting in metallic surface structures[20–22]. Laser-induced electrochemical de- and repassivation investigations are of interest in in-situ corrosion research studies[23–25]. The thermoemission of nonequilibrium electrons can be a unique technique for the generation of picosecond current pulses which cannot be realized by conventional instrumentation[17]. This allows short-lived intermediates of electrode reactions to be studied.

## Experimental

A block diagram of the laser-electrochemical system is depicted in Fig. 2. The electrochemical cell consists of a silver working microelectrode (μWE, $r_e$ = 15 μm radius) and a macroscopic platinum wire (1 mm diameter, 15 mm length) as counter electrode (CE). The fabrication of the extremely small μWE with a diameter of only 30 μm required an elaborate procedure described in the Supplementary information. A saturated Hg/$Hg_2SO_4$ reference electrode (not shown in Fig. 2) was employed to monitor the steady-state electrochemical potential during laser irradiation and the impedance spectroscopy (see below) experiments. Argon purged 0.2 M aqueous $K_2SO_4$ was used as the electrolyte with a pH adjusted to 2.2 with concentrated $H_2SO_4$.

Via a large-valued resistor ($R$: 1 MΩ), the μWE was kept at the desired steady-state potential $\varphi$, controlled by a digital-to-analog converter (DAQ; DAQPad-6020E DAC, National Instruments). In order to facilitate

measuring the small hot electron emission-induced signal $\Delta\varphi(t)$ (order of millivolts) on the dc-bias background $\varphi$, a high pass amplifier (HPA) was employed. It provided an input impedance of $10^{12}$ Ω, dc voltage suppression, an amplification of ~$10^2$, and a bandwidth of 1.5 MHz. The hot electron-induced transient potential change output $\Delta\varphi(t)$ of the HPA was recorded by a digital storage oscilloscope (OSC; WaveRunner 64Xi, LeCroy).

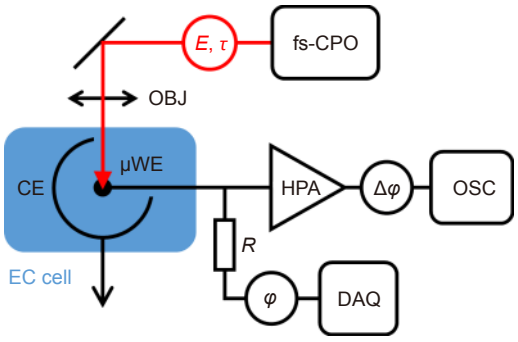


**Fig. 2 | Block diagram of the laser-electrochemical system.** μWE: silver working microelectrode; CE: platinum counter electrode; fs-CPO: femtosecond chirped pulse oscillator; $E$: laser pulse energy; $\tau$: pulse duration; OBJ: microscope objective; $R$: 1 MΩ resistor; DAQ: digital-to-analog converter output; $\varphi$: applied electrode potential; HPA: high pass amplifier; $\Delta\varphi$: transient voltage signal; OSC: digital storage oscilloscope.

A Ti:Sapphire Chirped Pulse Oscillator (fs-CPO; modified Femtosource XL, Femtolasers Produktions GmbH) delivered ultrashort pulses at a central wavelength of 800 nm ≙ 1.55 eV with a repetition rate of 11 MHz and pulse durations of either 55 fs or 213 fs. Pulses were picked with a Pockels cell at a rate of 50 Hz. The laser pulse energy $E$ was adjusted using a half-wave plate/polarizer combination and delivered through a microscope objective (OBJ; EC Plan-NEOFLUAR 10×/0.3, Zeiss). The laser beam exiting the microscope objective was characterized with a custom knife edge beam profiler[26], yielding a beam waist radius of $w_0 = (1.6 \pm 0.1)$ μm and a Rayleigh length of $z_R = (11.7 \pm 0.4)$ μm. Using the method reported in ref.[27], the μWE was placed in front of the beam waist to achieve a beam radius of $w = 10$ μm.

The applied laser peak fluences $F_0$ were varied between 30 mJ cm$^{-2}$ and 70 mJ cm$^{-2}$, well below (factor of ~6) the multi-pulse damage threshold of silver immersed in the electrolyte, as determined by the $A$–ln($E$) approach[28–30]. $\varphi$ was varied between −500 mV and +500 mV vs. the standard hydrogen electrode (SHE), which covers a potential region well within the polarizability range of the used silver microelectrode[31] as confirmed by repeated cyclic voltammetry sweeps.

## Results and discussion

Owing to the comparatively large time constant of the electrochemical cell, the measurable quantity is the integral of the emission current, i.e., the emitted charge (Eq. (4)) which is observable as the transient voltage change $\Delta\varphi(t)$ of the μWE. Figure 3 shows exemplary $\Delta\varphi(t)$ transients triggered by a fs laser pulse irradiating the μWE. The extracted peak voltage change of $\Delta\varphi_0 = (19.7 \pm 0.1)$ mV is highlighted in the inset of Fig. 3(a).

The electrons emitted from the electrode into the electrolyte get solvated and quickly reduce the solvent, i.e., reduce the solvated $H^+$ (hydronium ions). This leads to a recharging of the electrochemical double layer, characterized by its capacitance $C_{dl}$. That causes a transient change in the potential of the working electrode with amplitude $\Delta\varphi_0$. Thus, the emitted charge is $Q = \Delta\varphi_0\, C_{dl}$.

Impedance spectroscopy was employed for the determination of the double layer capacitance $C_{dl}(f, \varphi)$ as a

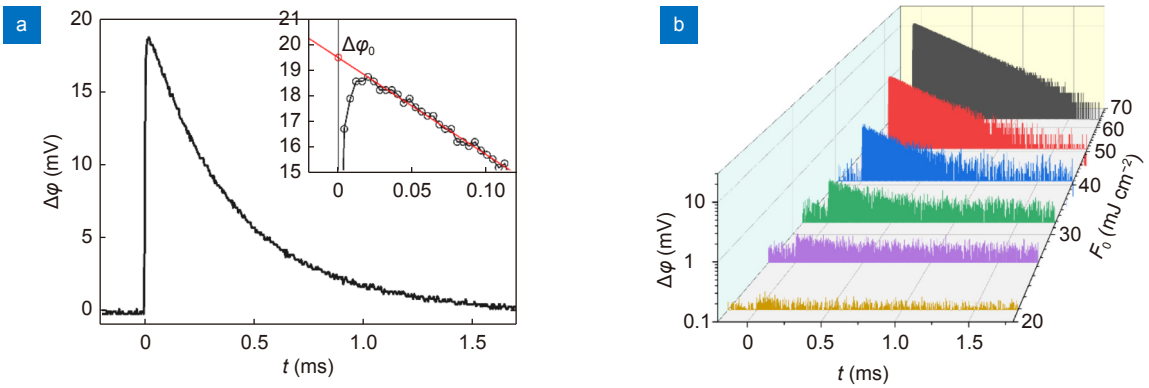


**Fig. 3 |** (**a**) Exemplary $\Delta\varphi(t)$ transient voltage measurement averaged over 100 single laser pulses. $\tau = (55 \pm 1)$ fs, $F_0 = (64 \pm 7)$ mJ cm$^{-2}$, $\phi = (-460 \pm 40)$ mV vs. SHE. The inset enlarges the region around $t = 0$ and shows the extracted peak voltage change $\Delta\varphi_0 = (19.7 \pm 0.1)$ mV. (**b**) Comparison of $\Delta\varphi(t)$ transient voltage measurements recorded at various laser peak fluences $F_0$.

function of frequency $f$ and the dc bias potential $\varphi$. Figure 4 shows an exemplary impedance trace measured *in situ* prior to recording the $\Delta\varphi(t)$ transient. Due to the large difference in surface area between the μWE and the CE (~$10^4$), the electrolyte and counter electrode contributions to the overall impedance can be neglected. To account for slight deviations from the ideal capacitive $1/f$ behavior (which is commonly observed in electrode impedance measurements), a constant phase element model (CPE)[32,33] was applied to determine $C_{dl}$. In this specific example, a frequency dependent double layer capacitance of $C_{dl}(f) = [(0.40 \pm 0.02)\ (f/1\ \text{Hz})^{(-0.064 \pm 0.003)}]$ nF was derived. For a frequency of 2.5 kHz, which approximates the inverse transient decay time of $\Delta\varphi(t)$, this translates to a capacitance of (0.21 ± 0.01) nF. This particular example ($\tau$ = (55 ± 1) fs, $F_0$ = (64 ± 7) mJ cm$^{-2}$, $\varphi$ = (−460 ± 40) mV vs. SHE) thus yields $Q$ = (4.2 ± 0.2) pC.

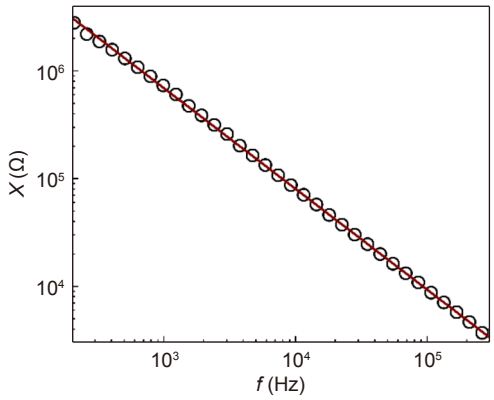


**Fig. 4 | Imaginary part *X* of an exemplary impedance measurement corresponding to the Δ*φ*(*t*) transient in Fig. 3.** The solid line shows the constant phase element fit.

Figure 5 shows the logarithmic plot of the emitted hot electron charge $Q$ over the applied electrode bias $\varphi$ and the peak laser fluence $F_0$ for two pulse durations, $\tau$ = (55 ± 1) fs and $\tau$ = (213 ± 1) fs. Despite the significant difference in terms of pulse duration (factor of ~4), emitted charges are largely unaffected. This also means that multiphoton excitation can be ruled out. The emitted charges range from 1 fC to 5 pC. This corresponds to 5×10$^3$ to 3×10$^7$ electrons emitted from the metal into the electrolyte solution. Thus, the external quantum efficiency is very low and ranges from 2×10$^{-8}$ to 6×10$^{-5}$. Considering the electron-phonon relaxation time (700 fs[34] for Ag) as the duration of the current pulse and the Gaussian beam area $w^2\pi$ as the emission surface, current densities exceeded 2×10$^6$ A cm$^{-2}$ [11,12,35].

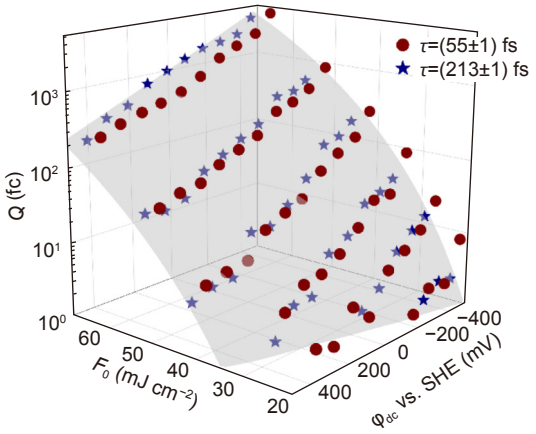


**Fig. 5 | Logarithmic plot of the emitted hot electron charge *Q* for two pulse durations, τ = (55 ± 1) fs (red circles) and τ = (213 ± 1) fs (blue stars), plotted over the applied electrode bias *φ* and peak laser fluence $F_0$.** The gray surface is calculated from Eq. (5) but for a constant factor with $\gamma_e$ = 62.8 J m$^{-3}$ K$^{-2}$, $\mu$ = 142 nm, $\beta$ = 0.15, and $\varphi_0$ = 3.41 eV at 0 V vs. SHE.

A comparison with previous work shows that the maximum charge density below the damage threshold of Ag is comparable with the present results, i.e., ca. 1 μC cm$^{-2}$ [11,12,35]. However, the method of the Gaussian beam radius determination strongly deviated which affects the reported intensity scale. The previous studies relied on the simple evaluation of the diameter of the blackened area on a photographic paper. This is known to overestimate the actual Gaussian beam radius. In the present work, it was determined by the accurate knife edge method[26,36].

The strongly superlinear, almost exponential, dependence of the emitted charge $Q$, and thus current density, on the laser fluence $F_0$ is in accordance with the thermoemission model expressed by Eq. (5). The two employed pulse durations are significantly shorter than the electron-phonon relaxation time (~ 700 fs[34]). With a weak temperature dependence of reflectivity and energy deposition depth, the local peak electron temperature $T_e$ will depend only on the local fluence $F(r)$ according to Eq. (2). The gray surface in Fig. 5 is calculated according to Eq. (5) using the following parameters. For silver, the work function in aqueous solution at the point of zero charge is 2.77 eV[37]. The point of zero charge is −640 mV vs. SHE[38]. With this, the work function is $\varphi_0$ = 3.41 eV at 0 V vs. SHE. The effective absorption length was reported as $\mu$ = 142 nm due to ballistic electron transport[8]. The electron heat capacity coefficient was reported to be $\gamma_e$ = 62.8 J m$^{-3}$ K$^{-2}$ [14]. For a moderately polished surface, a fraction of absorbed radiation of $\beta$ = 0.15 can be

assumed. On the other hand, the laser pulse durations had negligible impact on the emitted charge, which is incompatible with multiphoton emission.

The photonic excitation of the metallic Fermi sea leads to a broadened Fermi-Dirac distribution $n(\varepsilon)$ in the metal electrode (Fig. 6). The scale of $\varepsilon$ is opposite to the electrode potential scale $\varphi$. The electron transfer at the interface to the electrolyte takes place according to the Franck Condon principle at constant energy[39,40]. The Fermi level $\varepsilon_F$ in the absence of irradiation, which is electrochemically controlled by the applied potential $\varphi$, is positioned such that electron transfer to the electron scavenger in the electrolyte is thermodynamically negligible. The Fermi sea, which is heated upon laser irradiation, can inject electrons at a higher energy level than the equilibrium state into the fluctuating states of the hydronium ions. This corresponds to a more negative electrode potential $\varphi$. The initial reduction product of this process is hydrogen in statu nascendi, atomic $H^0$. According to the Franck Condon principle mentioned above, this extremely strong reducing agent can re-inject an electron into the metal. This became possible because the Fermi distribution returned to its equilibrium state after the electron-phonon relaxation.

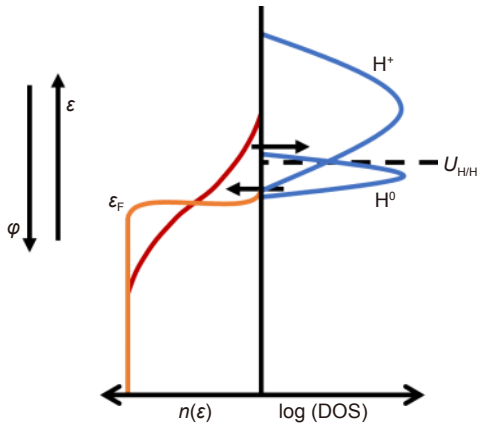


**Fig. 6 | Schematic electronic Fermi-Dirac distribution *n* on the metal and density of states (DOS) as function of the electronic energy *ε* of $H_3O^+$ and $H^0$.**

## Conclusions

Hot electrons in thermal nonequilibrium with the metal lattice were generated with low-energy photons from a femtosecond pulse laser. Two pulse durations, $\tau$ = (55 ± 1) fs and $\tau$ = (213 ± 1) fs significantly shorter than the electron-phonon relaxation time were employed with little effect on the emitted charge. A multiphoton emission scheme should depend strongly on intensity and thus pulse duration. This is however not observed, discouraging the interpretation of multiphoton photoemission. Electrons were emitted into an adjacent acidic $K_2SO_4$ electrolyte as giant current pulses with durations of the order of the electron-phonon relaxation time. Current densities reached $2\times10^6$ A cm$^{-2}$. Emitted electrons reacted with the solvent by reducing the protons to hydrogen. The transient electrode potential change based on the recharging of the electrochemical double layer was registered. The strongly superlinear dependence of the emitted charge on the laser fluence is supported by the thermoemission model. The photonic excitation of the metallic Fermi sea leads to a broadened Fermi-Dirac distribution in the metal electrode. The former injects electrons at a higher energy level, i.e., at a more negative electrode potential, than the equilibrium value into the fluctuating states of the hydronium ions. The reduction products can re-inject electrons into the metal because the Fermi distribution has returned to its equilibrium state.

## References

1. Hertz H. Ueber einen einfluss des ultravioletten lichtes auf die electrische entladung. *Ann Phys* **267**, 983–1000 (1887).
2. Lenard P. Ueber die lichtelektrische wirkung. *Ann Phys* **313**, 149–198 (1902).
3. Georges AT. Theory of the multiphoton photoelectric effect: a stepwise excitation process. *Phys Rev B* **51**, 13735–13738 (1995).
4. Girardeau-Montaut JP, Girardeau-Montaut C. Theory of ultrashort nonlinear multiphoton photoelectric emission from metals. *Phys Rev B* **51**, 13560–13567 (1995).
5. Damascelli A, Gabetta G, Lumachi A, Fini L, Parmigiani F. Multiphoton electron emission from Cu and W: an angle-resolved study. *Phys Rev B* **54**, 6031–6034 (1996).
6. Georges AT. High-order multiphoton photoelectric effect at midinfrared laser wavelengths. *Phys Rev A* **66**, 063412 (2002).
7. Bonn M, Denzler DN, Funk S, Wolf M, Wellershoff SS et al. Ultrafast electron dynamics at metal surfaces: competition between electron-phonon coupling and hot-electron transport. *Phys Rev B* **61**, 1101–1105 (2000).
8. Hohlfeld J, Wellershoff SS, Güdde J, Conrad U, Jähnke V et al. Electron and lattice dynamics following optical excitation of metals. *Chem Phys* **251**, 237–258 (2000).
9. Bäuerle D. *Laser Processing and Chemistry* (Springer, Berlin, 2011).
10. Anisimov SI, Kapeliovich BL, Perel'man TL. Electron emission from metal surfaces exposed to ultrashort laser pulses. *J Exp Theor Phys* **39**, 375–377 (1974).
11. Krivenko AG, Kautek W, Krüger J, Benderskii VA. Subpicosecond emission from mercury and silver into electrolyte solution: an experimental study. *Russ J Electrochem* **33**, 394–400 (1997).

12. Krüger J, Kautek W, Krivenko AG, Benderskii VA. Gigantic hydrogen-ion discharge currents initiated by a subpicosecond laser. *Russ J Electrochem* **34**, 1068–1075 (1998).
13. Kautek W, Armbruster O. Non-thermal material response to laser energy deposition. In Castillejo M, Ossi PM, Zhigilei L, eds. *Lasers in Materials Science* 43–66 (Springer, Cham, 2014).
14. Lin ZB, Zhigilei LV, Celli V. Electron-phonon coupling and electron heat capacity of metals under conditions of strong electron-phonon nonequilibrium. *Phys Rev B* **77**, 075133 (2008).
15. Ellison WJ, Lamkaouchi K, Moreau JM. Water: a dielectric reference. *J Mol Liq* **68**, 171–279 (1996).
16. Brodsky AM, Pleskov YV. Electron photoemission at a metal-electrolyte solution interface. *Prog Surf Sci* **2**, 1–73 (1972).
17. Benderskii VA, Benderskii AV. *Laser Electrochemistry of Intermediates* (CRC Press, Boca Raton, 1995).
18. Bockris JOM, Reddy AKN, Gamboa-Aldeco ME. *Modern Electrochemistry 2A*: *Fundamentals of Electrodics* 2nd ed (Springer, New York, 2000).
19. Benderskii VA, Efimov IO, Krivenko AG. Short-pulse laser activation of metal electrodes. *J Electroanal Chem Interfacial Electrochem* **315**, 29–64 (1991).
20. Tamir S, Zahavi J. Laser‐induced gold deposition on a silicon substrate. *J Vac Sci Technol A* **3**, 2312–2315 (1985).
21. Kautek W, Sorg N, Paatsch W. Laser-induced electrodeposition of transition metals on silicon. *Electrochim Acta* **36**, 1803–1810 (1991).
22. Sorg N, Kautek W, Paatsch W. Etching pretreatment and galvanic Cu enhancement of laser-deposited ultrathin Ni structures on p-Si. *Ber Bunsenges Phys Chem* **95**, 1501–1507 (1991).
23. Oltra R, Indrianjafy GM, Keddam M, Takenouti H. Laser depassivation of a channel flow double-electrode: a new technique in repassivation studies. *Corros Sci* **35**, 827–832 (1993).
24. Nagy TO, Pacher U, Giesriegl A, Soyka L, Trettenhahn G et al. Laser-induced electrochemical de- and repassivation investigations on plasma-oxidized aluminium alloys. *Appl Surf Sci* **302**, 184–188 (2014).
25. Nagy TO, Weimerskirch MJJ, Pacher U, Kautek W. Repassivation investigations on aluminium: physical chemistry of the passive state. *Z Phys Chem* **230**, 1303–1327 (2016).
26. Khosrofian JM, Garetz BA. Measurement of a Gaussian laser beam diameter through the direct inversion of knife-edge data. *Appl Opt* **22**, 3406–3410 (1983).
27. Armbruster O, Naghilou A, Pöhl H, Kautek W. *In-situ* and non-destructive focus determination device for high-precision laser applications. *J Opt* **18**, 095401 (2016).
28. Liu JM. Simple technique for measurements of pulsed Gaussian-beam spot sizes. *Opt Lett* **7**, 196–198 (1982).
29. Howard H, Conneely AJ, O'Connor GM, Glynn TJ. Investigation of a method for the determination of the focused spot size of industrial laser beams based on the drilling of holes in mylar film. *Proc SPIE* **4876**, 541–552 (2003).
30. Krüger J, Kautek W. Ultrashort pulse laser interaction with dielectrics and polymers. In Lippert TK, ed. *Polymers and Light* 247–290 (Springer, Berlin, 2004).
31. Pourbaix M. *Atlas of Electrochemical Equilibria in Aqueous Solutions* 2nd ed (National Association of Corrosion Engineers, Houston, 1974).
32. Brug GJ, van den Eeden ALG, Sluyters-Rehbach M, Sluyters J. The analysis of electrode impedances complicated by the presence of a constant phase element. *J Electroanal Chem Interfacial Electrochem* **176**, 275–295 (1984).
33. Pajkossy T. Impedance spectroscopy at interfaces of metals and aqueous solutions — surface roughness, CPE and related issues. *Solid State Ion* **176**, 1997–2003 (2005).
34. Groeneveld RHM, Sprik R, Lagendijk A. Femtosecond spectroscopy of electron-electron and electron-phonon energy relaxation in Ag and Au. *Phys Rev B* **51**, 11433–11445 (1995).
35. Krivenko AG, Krüger J, Kautek W, Benderskii VA. Subpicosecond-pulse-laser-induced electron emission from mercury and silver into aqueous electrolytes. *Ber Bunsenges Phys Chem* **99**, 1489–1494 (1995).
36. Krüger J, Kautek W. Ultrashort pulse laser interaction with dielectrics and polymers. In Lippert TK, ed. *Polymers and Light* 247–290 (Springer, Berlin, 2004).
37. Zolotovitskii YM, Korshunov LI, Benderskii VA. Electron work function from metals in a liquid dielectric. *Bull Acad Sci USSR, Div Chem Sci* **21**, 760–763 (1972).
38. Holze R. Table 3.1. Electrode potentials of zero charge of metal electrodes in contact with electrolyte solutions. In Lechner MD, ed. *Electrochemical Thermodynamics and Kinetics* 223–272 (Springer, Berlin, 2007).
39. Gerischer H. Über den ablauf von redoxreaktionen an metallen und an halbleitern. I. Allgemeines zum elektronenübergang zwischen einem festkörper und einem redoxelektrolyten. *Z Phys Chem* **26**, 223–247 (1960).
40. Gerischer H. Über den ablauf von redoxreaktionen an metallen und an halbleitern. II. Metall-elektroden. *Z Phys Chem* **26**, 325–338 (1960).

## Competing interests

The authors declare no competing financial interests.

## Supplementary information

Supplementary information is available for this paper at https://doi.org/10.29026/oea.2023.220170